



Seepage calculation method of loose rock mass under mining unloading

Fengjun Zhou^{a,b,*}, Jianhua Zhang^a

^a*School of Resources and Environment Engineering, Wuhan University of Technology, Wuhan 430070, China, email: hngcxzjf@163.com (F. Zhou)*

^b*School of Safety Engineering, Henan University of Engineering, Zhengzhou, 451191, China*

Received 19 July 2019; Accepted 19 December 2019

ABSTRACT

To explore the relationship between seepage coefficients of loose rock mass and mining unloading undermining unloading, the calculation method of seepage of loose rock mass undermining unloading is studied in depth. Weathered sandstone is used as a test sample, and a different size of axial pressure is applied to the specimen so that the specimen is subjected to different external forces to form different fissures of loose rock. The seepage-stress coupling model undermining unloading is constructed, and the relationship between fracture permeability coefficient and fracture closure is analyzed. The results show that the back pressure is proportional to the permeability coefficient of a loose rock mass. On this basis, according to the non-linear relationship between backpressure and fracture width during the mining unloading process, the specimen cracks during the mining unloading process are established. The relationship between the unloading permeability coefficient and mining unloading capacity of the loose rock mass is obtained by the equation of opening capacity and unloading capacity and the cubic law. The results show that the permeability coefficient increases slowly with the increase of mining unloading. When mining unloading increases to 60%–80%, the permeability coefficient increases rapidly. Moreover, the increase of mining unloading and pore water pressure of loose rock will also lead to an increase of permeability coefficient, which can play a dangerous early warning role in practical slope application.

Keywords: Mining unloading; Loose rock mass; Seepage calculation; Permeability coefficient; Fissures; Cubic law

1. Introduction

The problems of rock slope sliding, mine water inrush, surface subsidence and dam body instability in rock mass engineering are not only related to the stress state of Engineering structure, but also the role of water. Because of rock characteristics and tectonic action, there are a large number of cracks in a rock mass. These cracks form a complex fracture network in the rock mass, which together with rock blocks constitute a fractured rock mass [1]. Because the overflow of cracks in the rock mass is easy to expand, it becomes an important factor affecting the stability of engineering structures. In recent years, due to the need for geological hazard prevention and engineering safety evaluation,

a lot of work has been done on the coupling of seepage field and stress field in the rock mass, and considerable progress has been made. At present, the main hydraulic coupling model of the rock mass is the equivalent continuum model. There are more studies on the loading conditions, but less on the unloading or excavation conditions.

Because of the complexity of rock mass structure, the seepage of the rock mass is highly heterogeneous and anisotropic; rock mass fissure space is the main seepage channel of the rock mass, and rock mass fissure is significantly affected by stress environment. Therefore, the interaction between seepage and stress in the rock mass is a major feature of rock mass seepage [2]. It is difficult to give a reasonable explanation for this feature only by using the existing theory of groundwater dynamics. Especially in recent years, the construction of large reservoirs formed by high dams will have a great impact on

* Corresponding author.

the hydrological dynamics and groundwater in large areas. When the reservoirs impound and discharge water and concentrated rainfall, the fluctuation of the groundwater level will occur. Therefore, when the water level changes, the stability of the reservoir bank slope will also affect the safe operation of reservoirs. Landslides along reservoir banks are an important factor in the safety of cities and towns downstream [3]. Many scholars in China and abroad have studied the failure mechanism of this kind of slope. There are many studies on soil slope. Because of the complexity of rock slope, there are few studies. Especially when the water level is raked, there are few studies on the changes in groundwater level and seepage flow. But this problem is the key to the stability of the reservoir bank slope. The key factors, its mechanism, especially why it developed into a large-scale landslide, still have many unknown points.

Accordingly, she proposed a lumped parameter model and a continuum model, an equivalent continuum model, a fracture network model and a dual medium model for the coupling of seepage field and stress field in a rock mass. Lan believes that because of the existence of cracks in the rock mass, the change of groundwater level will change the pressure of pore water in the rock mass, thus affecting the deformation and failure of rock [4]. Under the human engineering activities, on the one hand, the excavation of the project causes the unloading of the rock mass by mining, and at the same time, the engineering load is applied on the rock mass, changing the distribution of the stress field inside the rock mass, affecting the structure of the rock mass, resulting in the change of groundwater behavior and groundwater mechanics characteristics in the rock mass [5]; on the other hand, because of the emergence of engineering bodies, the conditions of recharge, runoff, and discharge of regional or local groundwater are changed, and the seepage field of groundwater under artificial disturbance is formed. The strength, scope and form of mechanical action of groundwater on rock mass also change, which ultimately affects the stability of rock mass [6–8]. In the mining process, many rock mass deformations are related to the seepage pressure of groundwater in the rock mass. Often, due to the interaction of mining stress, in-situ stress and groundwater seepage force in the mine, underground water inrush [9] occurs. The reason is that the unloading effect of underground mining results in the deformation of the rock mass increases the width of cracks in the surrounding rock, changes the permeability of rock mass, and changes the physical and mechanical properties of the rock mass, leading to accidents. In this paper, the seepage calculation method of loose rock mass undermining unloading is analyzed experimentally, and the relationship between unloading permeability coefficient of loose rock mass and mining unloading quantity is analyzed accurately.

2. Materials and methods

2.1. Test subjects

The rock sample belongs to the Middle Jurassic, weathered sandstone. The sample is cylindrical, with a diameter of 39 mm and a height of 80 mm. The stress path adopted in the test is to exert axial pressure on rock specimen to near yield state, and then unload [10] to simulate various stress effects experienced by rock slope undermining load [11]. The basic physical and mechanical parameters of rock samples are shown in Table 1.

2.2. Test method

Firstly, the specimen is subjected to axial pressure, which gradually increases to a stress level of 1 MPa before failure, and remains unchanged for 30 min; then, the confining pressure is 800 KPa (equivalent to the self-weight geotechnical pressure in the depth of 40 m). After 30 min, the rock mass is stabilized for 30 min under this stress state, and a certain water head is considered. With 100, 200 and 300 KPa, the specimens were stabilized for 30 min, then the confining pressure was unloaded, and the seepage rate was measured simultaneously [12]. Each pole is unloaded at 100 KPa with a time interval of 30 min.

As shown in Fig. 1, the permeability coefficient increases with the increase of unloading capacity, but it does not change much in the elastic stage of unloading; when the plastic stage of unloading is entered, the permeability coefficient changes greatly, especially when the unloading capacity reaches 80% of the ultimate unloading capacity, the permeability coefficient increases rapidly [13,14]. It can be seen that the plastic deformation of rock mass has a great influence on the permeability coefficient. It shows that when rock mass enters the unloading plastic stage, the micro-cracks formed by unloading of rock mass have gradually become a smooth seepage path. At the same time, it can be seen that the permeability coefficient is proportional to the unloading amount when the pore water pressure is low [15]. With the increase of pore water pressure, the permeability coefficient increases greatly under the same unloading amount.

2.3. Coupled seepage-stress model undermining unloading

2.3.1. Effect of back pressure on the permeability coefficient of loose rock mass

The main factors affecting seepage in loose rock mass are porosity of rock mass and fracture width [16]. When the external stress environment changes, the fissures of loose rock mass will change, and then the permeability characteristics of loose rock mass will change greatly.

Table 1
Basic physical and mechanical parameters of rock samples

Name of parameter	Poisson ratio	Modulus of elasticity/GPa	Water content/%	Proportion	Saturation density/g cm ⁻³	Porosity/%
Numerical value	0.34	0.489	10.1	2.656	2.265	22.84

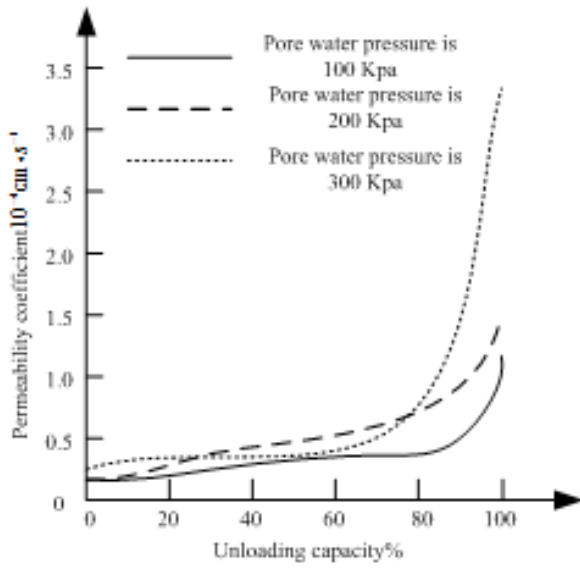


Fig. 1. Relation of permeability coefficient and unloading level under different conditions.

Generally, the permeability of loose rock mass is dominated by fissures, and the fissures are controlled by the roughness and width of the fissures. At the same time, the geometric roughness of the fissure surface is closely related to the stress field. When the external force field changes, the strength of the fissures is low and the deformation is large, so the roughness and width of the fissure surface will follow. Change [17] will lead to changes in fracture permeability characteristics; on the other hand, when the osmotic pressure is large, it will also have an impact on fracture mechanical behavior.

For porous and fractured media, the permeability coefficient can be expressed as:

$$k = \frac{\gamma_w (b + s \Delta \epsilon)^3}{12 \mu s} \tag{1}$$

Among them, s is the spacing of cracks; b is the opening of cracks; $\Delta \epsilon$ is the strain of vertical cracks; γ_w is the gravity of water, and μ is the coefficient of fluid viscosity.

When the stress in the vertical direction of the fracture changes to $\Delta \sigma$, the total displacement is as follows:

$$\Delta u = \Delta u_s + \Delta u_f = \left[\frac{s}{E} + \frac{1}{k_n} \right] \Delta \sigma \tag{2}$$

Among them, Δu is the total displacement, Δu_s is the pore displacement, Δu_f is the fracture displacement, k_n is the fracture normal stiffness [18].

The fracture displacement vector is:

$$\Delta u_f = \Delta \epsilon \left[\frac{k_n}{E} + \frac{1}{s} \right]^{-1} \tag{3}$$

The hydraulic permeability coefficient of a single fracture is:

$$k = k_0 \left(1 + \Delta \epsilon \left[\frac{k_n b_0}{E} + \frac{b_0}{s} \right]^{-1} \right)^3 \tag{4}$$

Since the width b of the fracture is $b_0 \ll s$ compared with the spacing of the fracture, the upper formula can be changed to:

$$k = k_0 \left(1 + \Delta \epsilon \left[\frac{k_n b_0}{E} \right]^{-1} \right)^3 \tag{5}$$

After simplification, the upper form becomes:

$$k = k_0 \left(1 + \frac{\Delta b}{b_0} \right)^3 \tag{6}$$

Eq. (6) reflects the relationship between the fracture permeability coefficient and the fracture closure of loose rock mass under backpressure, and the fracture closure is the result of back pressure [19–22]. Therefore, Eq. (6) reflects the effect of back pressure on the fracture permeability coefficient, and the larger the fracture width of loose rock, the larger the permeability coefficient.

2.3.2. Relationship between unloading permeability coefficient and unloading quantity

For the stress loading process, the relationship between macro-cracks and their multiple back pressures has been studied by many scholars. For example, Goodman (1976) proposed the relationship between backpressure and closure of a single fracture surface [23–25]:

$$\sigma_n = \sigma_{ni} + R \sigma_{ni} \left(\frac{\Delta b}{\Delta b_{max} - \Delta b} \right)^t \tag{7}$$

Among them, σ_n is the backpressure of fracture surface; σ_{ni} is the initial back pressure of fracture surface; Δb is the closure of fracture surface; Δb_{max} is the maximum closure of fracture surface [26,27]. R and t are both experimental parameters and constant values.

By combining Eq. (7) with Eq. (6), the relationship between permeability coefficient and stress variation under loading can be obtained.

$$\frac{k}{k_0} = \frac{I}{(I + A)^3} \tag{8}$$

Among them, $A = (\sigma_n - \sigma_{ni} / R \sigma_{ni})^{1/t}$, and A is the material constants of a loose rock mass.

Based on a series of studies on the permeability coefficient and backpressure of a single fracture, Barton considers that roughness and width of the fracture surface will affect the permeability coefficient for a single fracture surface.

When the stress acts on a single fracture, the fracture surface closes, and the size of the closure will affect the permeability coefficient. Based on the experimental results, the relationship between the backpressure and the fracture closure [28] is obtained. On this basis, a hyperbolic model of the fracture surface is proposed.

$$\sigma_n - \sigma_{ni} = \frac{\Delta b}{\alpha - \beta \Delta b} \tag{9}$$

α and β are experimental constants.

It can be seen from Fig. 1 that the variation curve of fracture surface closure with normal stress is different in the process of loading and unloading. There is a hysteretic effect in the process of loading and unloading, that is, in the process of loading and unloading, the closure of fracture surface in the process of loading and unloading is different from that in the process of unloading. There are differences in the opening of the aggregate.

Because of the nonlinearity between stress and crack width during unloading, the relationship equation between crack opening and unloading is established.

$$\sigma_n = \sigma_{ni} - R\sigma_{ni} \left(\frac{\Delta b}{b_{ini} + \Delta b} \right)^\eta \tag{10}$$

Then:

$$\frac{\sigma_{ni} - \sigma_n}{\sigma_{ni}} = R \left(\frac{\Delta b}{b_{ini} + \Delta b} \right)^\eta \tag{11}$$

Among them, σ_n is the positive effective stress at a certain time; σ_{ni} is the initial positive effective stress at the fracture surface; the variation of fracture surface opening is Δb ; b_{ini} is the opening of fracture surface under the initial stress σ_{ni} ; R and η are the test coefficients.

Thus, from Eq. (11), it can be obtained that:

$$\Delta b = \frac{(\zeta / R)^\frac{1}{\eta} b_{ini}^\frac{1}{\eta}}{1 - (\zeta / R)^\frac{1}{\eta}} \tag{12}$$

Among them, $\zeta = \sigma_{ni} - \sigma_n / \sigma_{ni}$ is the effective stress unloading ratio.

Since the change of the permeability coefficient is mainly caused by the change of fracture width, it is assumed that the initial permeability coefficient of the rock mass is K_0 and the fracture width is b_0 . According to the law of cube [29,30], there are:

$$K_0 = \frac{8b_0^3}{12\mu s} \tag{13}$$

For loose rock mass, there are:

$$\frac{K}{K_0} = \left(1 + \frac{\Delta b}{b_0} \right)^3 = \left(1 + \frac{(\zeta / R)^\frac{1}{\eta}}{(1 - (\zeta / R)^\frac{1}{\eta})} \right)^3 = \frac{1}{\left(1 - (\zeta / R)^\frac{1}{\eta} \right)^3} \tag{14}$$

Eq. (14) is the relationship between the unloading permeability coefficient of loose rock mass and mining unloading.

3. Results

3.1. Survey of research areas

The unexploited slope as shown in Fig. 2 is the research area, and the mechanical index of the slope is shown in Table 2. The x , y and z of the whole coordinate system correspond to the geographic normal east, normal north and vertical upward respectively. The slope is 100 m long in East and West, 20 m wide in South and north, and 50 m high in height. There are two large faults in the slope. The width of one fault is 0.1 m in East and West direction, the other is north and south direction, and the dip angle is 30 degrees. These faults are simulated as the main faults. There are also three groups of orthogonal joints, which are perpendicular to the x , y and z coordinate axes respectively. Because the permeability principal axis coincides with the coordinate axis, the equivalent continuum model is used to simulate the loose rock mass. The three principal values of the equivalent permeability tensor are 10×10^{-6} m/s, and the permeability principal directions are parallel to the x , y and z coordinate axes.

3.2. Relationship between the permeability coefficient and unloading under different back pressure

Table 3 is the test results of the permeability coefficient and mining unloading under different backpressure. The relationship between permeability coefficient and unloading under different back pressure during the unloading process of loose rock is shown in Fig. 3. From the graph, it can be seen that with the increase of unloading amount, the permeability coefficient increases slightly in the initial stage, but when the unloading amount reaches 60%–80%, the permeability coefficient increases rapidly. It shows that after the unloading amount reaches 60%–80%, the micro-cracks in



Fig. 2. Overview of the research area.

Table 2
Mechanical parameters of slope rock masses

Rock stratum	Severe/ KN m^{-3}	Modulus of elasticity/GPa	Poisson ratio	Cohesive force/MPa	Internal friction angle/(°)
Rock	27	21	0.18	1	40
Fault	2	10	0.23	0.5	40

Table 3
Test result of permeability during unloading

Pore pressure 100 KPa		Pore pressure 200 KPa		Pore pressure 300 KPa	
Mining unloading capacity (100%)	Permeability coefficient ratio (k/k_0)	Mining unloading capacity (100%)	Permeability coefficient ratio (k/k_0)	Mining unloading capacity (100%)	Permeability coefficient ratio (k/k_0)
0.00	1.00	0.00	1.00	0.00	1.00
14.29	1.00	16.67	1.01	20.00	1.00
28.57	1.05	33.33	1.07	40.00	1.08
42.86	1.10	50.00	1.03	60.00	1.16
57.14	1.16	66.67	1.35	80.00	1.98
71.73	1.38	83.33	2.58	90.00	3.91
85.71	2.42	91.67	5.68	98.00	8.62
98.57	11.78	98.33	8.54	—	—

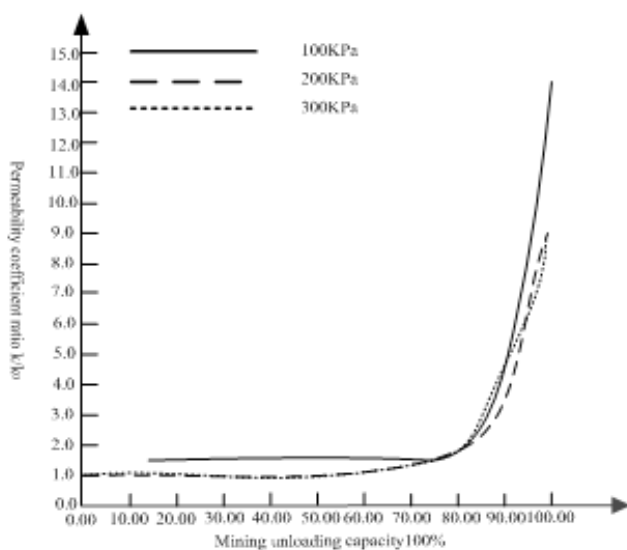


Fig. 3. Relationship between the permeability coefficient and unloading capacity of loose rock under different back pressure during the unloading process.

loose rock mass have gradually expanded and connected, forming a seepage channel, which makes the rock mass seepage. The permeability coefficient began to increase rapidly. Comparing the test results of 100, 200, and 300 KPa with backpressure, it is found that with the increase of backpressure, the unloading amount required for the rapid increase of permeability coefficient is smaller; when the backpressure is low, there is no gradual increase process, that is, the lower

the backpressure, the stronger the mutation of permeability coefficient. With the development of unloading, the difference between the highest and lowest permeability coefficient is about 10 times.

3.3. Analysis of permeability coefficient change at a certain unloading volume

Table 4 shows the test results of the permeability coefficient of loose rock changing with pore pressure while unloading quantity remains stable. Figs. 4a and b show the relationship curve between pore pressure and permeability coefficient in the process of loading and unloading pore water pressure under certain unloading quantity. It can be seen from the graph that with the increase of pore water pressure, the permeability coefficient of rock also increases; when pore water pressure is unloaded, the permeability coefficient of rock does not decrease along the original path, but forms a hysteretic loop composed of permeability coefficient; the permeability coefficient of pore water pressure during unloading is lower than that under loading, which is due to the change of pore water pressure. The change in effective stress has a certain effect on the formation of rock permeability. During the loading and unloading cycle of pore water pressure, the cyclic change of effective stress exerted on rock leads to that the final fracture width is smaller than the original one, so after unloading of pore water pressure, the permeability coefficient of rock cannot be restored to the state before the change of water pressure. Comparing the curves of 25% and 37.5% unloading capacity, it can be seen that the higher the unloading capacity is, the faster the permeability coefficient increases with the increase of pore water pressure.

Table 4
Test result of permeability during pore pressure loading and unloading

Unloading capacity 25%		Unloading capacity 37.5%	
Backpressure (KPa)	Permeability coefficient ratio (k/k_0)	Backpressure (KPa)	Permeability coefficient ratio (k/k_0)
100+	1.000	100+	1.083
200+	1.009	200+	1.112
300+	1.009	300+	1.150
200–	1.005	200–	1.091
100–	0.968	100–	1.046
200+	0.978	200+	1.058
300+	0.993	300+	1.117
200–	0.965	200–	1.049
100–	0.914	100–	1.003

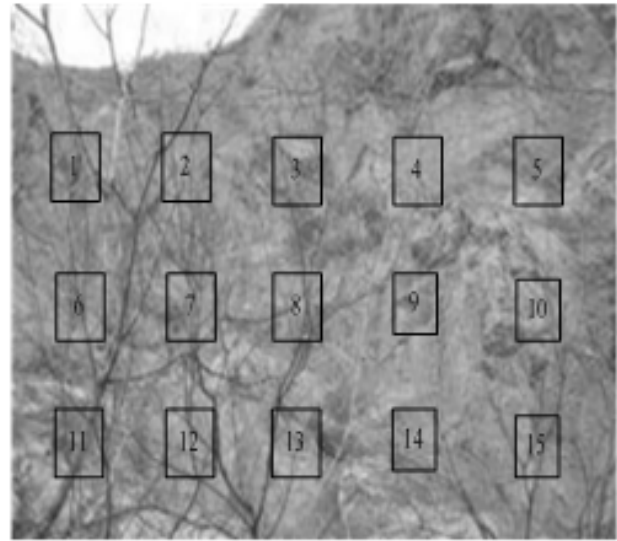


Fig. 5. General situation of mining area II.

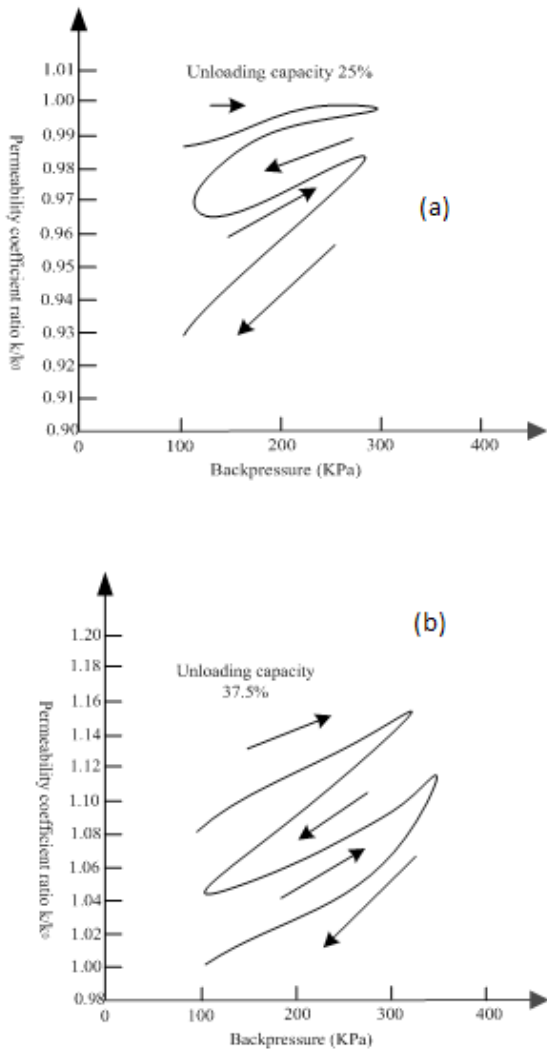


Fig. 4. Relationship curve between pore pressure and permeability coefficient during loading and unloading of pore water pressure at (a) 25% unloading capacity and (b) 37.5% unloading rate.

3.4. Application effect analysis

Based on the above experimental results, the practical application value of this method is analyzed. The accuracy of seepage calculation of loose rock around the mining slope is of great value to the mining of ore bodies. Therefore, two mining areas are selected as the experimental research areas in the experiment. The second survey is as follows: Xinli mining area is located in Laizhou Bay. Coastal plain area, the mining area is low-lying and flat, the elevation of the surface is generally 1.2–4.5 m, Sanshan Island-Cangshang fault is the ore-controlling structure in this area. The fault is located at the west end of the Jiaodong gold mineralization concentration area. It starts from Sanshan Island in the north-east and goes to Jiawuzi in the south-west. The two ends extend into the Bohai Sea. The southwest end of the fault is exposed to Fulong Island after it enters the sea. The fault zone is only partially exposed to the surface, most of which are covered by the quaternary system. The land outcrop is about 12 km long and 50 m to 200 m wide. It is S-shaped in-plane, with an overall strike of 40° and a local strike of 70° to 80°. It tends to SE with an inclination of 45° to 75°. The main fracture surface is gentle and wavy. It belongs to a torsional fracture. The main fracture surface develops a gray-black fault gouge of 50 to 100 mm. The lithology is yellow iron sericite granite. Cracks are not well developed in the orebody. Cracks are well developed in the roof rock mass of the orebody, most of which are moist areas, and there are many dripping points and some sprinkling points. The second general situation of the mining area is shown in Fig. 5.

This paper analyses the validity of the seepage calculation method of loose rock mass undermining unloading. To highlight the high application value of this method, the permeability coefficient calculation method of well water pumping test and the permeability coefficient calculation method of coarse-grained soil based on pore size is used as an experimental comparison, and the expert evaluation method is used in the experiment. Applying the percentile

Table 5
Evaluation of three methods in the first research area

Research location	Method in this paper			Well water pumping test			Coarse-grained soil method based on pore size		
	Security early warning performance	Accuracy of crack width calculation	Permeability of rocks	Security early warning performance	Accuracy of crack width calculation	Permeability of rocks	Security early warning performance	Accuracy of crack width calculation	Permeability of rocks
1	98.6	98.4	98.4	68.5	72.3	65.8	62.3	56.2	56.3
2	93.5	96.5	96.5	65.6	71.5	66.8	65.2	55.4	54.2
3	97.5	94.8	97.5	75.2	65.3	59.3	54.6	52.3	55.4
4	98.5	97.2	95.8	68.5	65.6	72.5	56.5	57.6	55.8
5	98.4	96.5	96.8	74.5	66.5	65.4	58.3	54.1	54.6
6	97.6	94.8	97.5	65.8	67.1	54.6	63.2	52.3	53.6
7	98.6	98.2	98.4	65.4	71.4	72.3	64.2	52.3	54.2
8	98.6	99.5	98.8	66.2	72.5	77.6	65.3	51.4	56.2
9	95.2	95.2	95.2	62.3	65.3	71.2	62.3	52.3	55.2
10	94.6	93.6	96.2	64.4	65.3	72.3	64.6	54.5	54.3
11	93.8	94.6	94.2	65.3	67.5	74.3	64.6	54.3	56.3
12	92.6	95.2	93.6	63.5	68.2	73.5	54.2	55.4	52.1
13	94.5	92.3	94.5	64.2	71.2	74.5	57.3	52.4	54.3
14	95.6	92.3	95.6	65.3	65.3	68.5	58.3	55.4	57.2
15	97.7	96.9	97.5	68.7	69	66.8	61.2	53.9	55.2

system to evaluate the application effect of the three methods in the three research areas, eight loose rock areas in the three research areas were selected to evaluate. The evaluation factors include the safety warning performance of the three methods, the accuracy of crack width calculation and the permeability of the rock, and the experiments. The expert evaluation results of the three methods in the three research areas are described in Tables 5 and 6 respectively.

The results of Tables 5 and 6 show that the method has good safety warning performance, crack width calculation accuracy and rock permeability in the study area. The expert evaluation score is above 90, but the calculation method of permeability coefficient in well water pumping test and the calculation of the permeability coefficient of coarse-grained soil based on pore size is better. The safety early warning performance, crack width calculation accuracy and rock permeability score of the first application area of the method are much lower than those of the method in this paper. It shows that the method in this paper has good practical effect and can play an early warning role for the safety of the research area, and the calculated crack width value is accurate and the estimation effect of rock permeability is good. It is a high-quality permeability calculation method.

4. Discussions

In this paper, the cylindrical weathered sandstone is taken as the test object, and the Fenghua rock is formed into a loose rock by loading different axial pressures on the specimen. The seepage-stress coupling model undermining unloading is used to analyze the influence of back pressure on the permeability coefficient of loose rock mass and the

relationship between unloading permeability coefficient and unloading quantity. The permeability coefficient and mining of loose rock are obtained. The experimental results show that the permeability coefficient of loose rock increases rapidly when the mining unloading amount reaches 60%–80%. At this time, the micro-cracks in loose rock mass expand and connect to form seepage channels, so the permeability coefficient begins to increase rapidly. The experimental results under different back pressures show that with the increase of backpressure, the permeability coefficient increases, but the unloading capacity is small. When the unloading quantity is constant, the pore water pressure increases and the permeability coefficient increases. Compared with the Figs. 4a and b of 25% and 37.5% unloading quantity, it can be seen that the higher the unloading quantity is, the faster the permeability coefficient increases with the increase of pore water pressure.

Coupled analysis of the stress field and seepage field in loose rock mass undermining unloading is a huge and complex research project, which involves many disciplines. This paper has only done a small part of exploration work based on the previous research results, and some conclusions need to be further verified and developed in the future. Combining with the work of this paper, the following problems can be studied emphatically: this paper considers the permeability characteristics of mining unloading loose rock mass under the condition of crack, while the permeability characteristics of unloading rock mass under the condition of multi-crack or even fracture network need to be further studied; because of the limitation of conditions, it is impossible to obtain the rock fracture in the process of seepage test. The evolution of the gap in a direction that needs to be studied in the future.

Table 6
Evaluation of three methods applied in the second research area

Research location	Method in this paper			Well water pumping test			Coarse-grained soil method based on pore size		
	Security early warning performance	Accuracy of crack width calculation	Permeability of rocks	Security early warning performance	Accuracy of crack width calculation	Permeability of rocks	Security early warning performance	Accuracy of crack width calculation	Permeability of rocks
1	99.2	99.5	99.9	65.2	54.2	52.3	62.5	63.2	62.3
2	98.6	99.4	99.8	63.5	53.6	54.2	63.5	62.5	65.3
3	99.6	99.5	99.6	64.1	51.6	55.3	64.5	64.5	64.5
4	99.5	99.7	99.7	52.3	55.3	51.2	65.2	68.5	63.5
5	99.2	99.1	99.8	62.5	55.2	53.6	66.1	63.5	61.5
6	99.3	99.2	99.5	54.6	56.2	52.1	62.3	64.2	64.5
7	99.5	99.2	99.6	53.6	54.7	54.5	65.3	63.5	62.3
8	99.7	99.2	99.7	51.4	55.3	57.2	66.2	64.5	65.3
9	99.2	99.5	99.2	52.3	54.2	52.4	62.5	65.4	62.3
10	99.0	99.4	99.5	55.4	53.1	54.7	64.5	63.5	64.2
11	99.1	99.7	99.4	51.3	55.6	56.2	62.3	66.4	67.1
12	99.5	99.3	99.6	52.3	55.7	58.3	63.5	62.5	62.3
13	99.6	99.5	99.8	5.6	55.8	54.6	65.3	66.2	63.5
14	94.5	99.0	99.2	54.6	52.3	51.2	65.4	63.5	66.5
15	99.3	99.3	99.7	58.4	54.5	53.8	64.5	64.3	63.7

5. Conclusions

At present, the study of seepage in the rock mass is still based on loading rock mechanics, but different rock mass engineering has different mechanical conditions. Under different mechanical conditions, rock mass has different mechanical properties. Therefore, for engineering which belongs to unloading mechanics in the mechanical category, the method of loading rock mechanics in advance is also used. It is very difficult to solve practical engineering problems, but it may also cause huge losses to the project. Therefore, for the study of seepage in unloaded rock mass engineering, the relationship between unloading mechanics and seepage mechanics should be further clarified by considering the influence of normal or tangential forces on the fracture surface of unloaded rock mass and coupling method between unloading mechanics and seepage mechanics. Therefore, the coupling model of the seepage field and unloading stress field in the loose rock mass is established based on the combination of field data acquisition, theoretical analysis and simulation test, theoretical analysis as a means, simulation test as verification and correction of the technical route.

References

- [1] W. Zhang, B. Dai, Z. Liu, C. Zhou, Modeling free-surface seepage flow in complicated fractured rock mass using a coupled RPIM-FEM method, *Transp. Porous Media*, 117 (2017) 443–463.
- [2] C. Chai, Y. Su, L. Yang, Seepage rate function establishment and validation for trapezoidal canal based on piping head ponding test, *Trans. Chin. Soc. Agric. Eng.*, 33 (2017) 91–95.
- [3] Y.L. Wang, Z. Zhuo, Z.L. Liu, Finite element analysis for inclined wellbore stability of transversely isotropic rock with HMCD coupling based on weak plane strength criterion, *Sci. China Technol. Sci.*, 60 (2017) 138–151.
- [4] T. Lan, C. Fan, H. Zhang, A.S. Batugin, L. Ruibin, Y. Yang, C. Jia, Seepage law of injected water in the coal seam to prevent rockburst based on coal and rock system energy, *Adv. Civ. Eng.*, 2018 (2018) 1–9.
- [5] G.H. Yu, Y. Hui, D.L. Gao, Calculation of isotope shift of Mg⁺⁺ ion by using the relativistic multi-configuration interaction method, *Acta Phys. Sin.*, 63 (2018) 151–163.
- [6] Z. Liu, A. Baghban, Application of LSSVM for biodiesel production using supercritical ethanol solvent, *Energy Sources Part A*, 39 (2017) 1869–1874.
- [7] Z. Liu, W. Peng, M. Motahari-Nezhad, S. Shahraki, M. Beheshti, Circulating fluidized bed gasification of biomass for flexible end-use of syngas: a micro and nanoscale study for production of bio-methanol, *J. Cleaner Prod.*, 129 (2016) 249–255.
- [8] W. Tang, J. Hong, X. Huang, Meticulous simulation and evaluation of seepage control effects at right bank dam foundation and an underground powerhouse of Jinping I hydropower station, *IOP Conf. Ser.: Earth Environ. Sci.*, 189 (2018) 022021.
- [9] W.Q. Zhang, J.D. Yuan, Z.C. Wang, An experimental study on compressive shear seepage laws of a mining-induced fractured rock mass, *Rock Soil Mech.*, 38 (2017) 2473–2479.
- [10] G.X. Zhang, Study on numerical simulation method used in analyzing the effect of seepage pressure in continuous medium with pores on deformation and stress, *J. Hydraul. Eng.*, 48 (2017) 640–650.
- [11] Z. Wang, Y. Glais, L. Qiao, Hydro-geochemical analysis of the interplay between the groundwater, host rock and water curtain system for an underground oil storage facility, *Tunnelling Underground Space Technol.*, 71 (2017) 466–477.
- [12] X. Zhang, C. Wu, T. Li, Comparison analysis of fractal characteristics for tight sandstones using different calculation methods, *J. Geophys. Eng.*, 14 (2017) 120–131.
- [13] H. Wang, X. An, Z. Zhang, Effect of advanced treatment on ammonia nitrogen contained in secondary effluent from wastewater treatment plant, *Fresenius Environ. Bull.*, 27 (2018) 2043–2050.
- [14] Y. Han, C. Zhou, Y. Fan, A new permeability calculation method using nuclear magnetic resonance logging based on pore sizes:

- a case study of bioclastic limestone reservoirs in the A oilfield of the Mid-East, *Pet. Explor. Dev.*, 45 (2018) 183–192.
- [15] Y. Guan, X. Zhao, G. Wang, 3D dynamic numerical programming and calculation of vertical buried tube heat exchanger performance of ground-source heat pumps under coupled heat transfer inside and outside of tube, *Energy Build.*, 139 (2017) 186–196.
- [16] J. Yao, H. Tao, Z.Q. Huang, Numerical simulation of ferrofluid flow in porous media under coupled magnetic and seepage fields, *Chin. Sci. Bull.*, 62 (2017) 836–846.
- [17] H. Li, Y. Wang, J. Liu, Computational model for production of a rhombus reverse five-point well pattern with non-darcy seepage, Taking into account startup pressure gradient, *Chem. Technol. Fuels Oils*, 53 (2017) 1–6.
- [18] D.H. Jiang, H.T. Lin, A summary of key techniques research on resource allocation in cloud computing environment, *J. China Acad. Electron. Inf. Technol.*, 13 (2018) 82–88.
- [19] J. Zhao, J.G. Zhang, Z.H. Liu, Calculation method of lightning induced voltage of shielded cable in substation, *J. Power Supply*, 15 (2017) 167–172.
- [20] A. Amamra, K. Khanchoul, Water quality of the Kebir watershed, Northeast of Algeria, *J. Clean Was*, 3 (2019) 28–32.
- [21] M.L. de Menezes, G. Johann, A. Diorio, N.C. Pereira, E.A. Da Silva, Phenomenological determination of mass transfer parameters of oil extraction from grape biomass waste, *J. Cleaner Prod.*, 176 (2018) 130–139.
- [22] F. Halek, A. Kavousi-Rahim, Influence of antioxidant addition on the emissions of a diesel engine by using waste cooking oil biodiesel, *Energy Environ.*, 29 (2018) 732–741.
- [23] P. Kumar, V. Joshi, A geospatial- statistical approach to alienate priority area of upper watershed of River Subarnarekha using morphometric assessment framework, *Malaysian J. Geosci.*, 3 (2019) 21–31.
- [24] B. Brika, H. Ghuila, H. Mosbah, Municipal water shortage, and related water issues in the City of Tajoura: a case study to raise public awareness, *Water Conserv. Manage.*, 2 (2018) 31–33.
- [25] H.B. Kang, Y.S. Liu, Y.N. Qu, Intelligent diagnostic system of micro-net in a cloud computing environment, *Chin. J. Power Sources*, 41 (2017) 486–488.
- [26] Ogunkunle, T. Joseph, Adewumi, Aderiike, Adepoju, A. Olufemi, Biodiversity: overexploited but an underutilized natural resource for human existence and economic development, *Environ. Ecosyst. Sci.*, 3 (2019) 26–34.
- [27] P.R. Qiu, X.P. Yuan, S. Gan, Research on QR code generation and recognition technology based on android platform in instrument equipment management system of colleges and universities, *Autom. Instrum.*, 38 (2018) 67–70.
- [28] J.J. Sun, Y. Zhao, S.G. Wang, Improvement of SIFT feature matching algorithm based on image gradient information enhancement, *J. Jilin Univ. (Sci. Ed.)*, 56 (2018) 82–88.
- [29] S.A. Hosseini, F. Sharifi, Improvement stability of earth canal banks using geotechnical approaches, *Geol. Ecol. Landscapes*, 3 (2019) 308–317.
- [30] B.M. Qiang, X. Wu, P. Wu, Research on load strength optimization design of bridge structure in bridge crane, *Comput. Simul.*, 34 (2017) 178–183.